Materials Science & Engineering A 720 (2018) 231–237

Contents lists available at ScienceDirect

Materials Science & Engineering A

journal homepage: www.elsevier.com/locate/msea

Enhancing strength and thermal stability of TWIP steels with a heterogeneous structure

T. Xiong[a,b], S.J. Zheng[a,*], Y.T. Zhou[a], J.C. Pang[a], Q.Q. Jin[a], H.L. Ge[a,b], X.D. Zheng[a,b], L.X. Yang[a], I.J. Beyerlein[c], X.L. Ma[a,d,**]

[a] Shenyang National Laboratory for Materials Science, Institute of Metal Research, Chinese Academy of Sciences, 72 Wenhua Road, Shenyang 110016, PR China
[b] School of Material Science and Engineering, University of Science and Technology of China, Heifei 230026, PR China
[c] Mechanical Engineering Department, Materials Department, University of California at Santa Barbara, Santa Barbara, CA 93106, USA
[d] School of Material Science and Engineering, Lanzhou University of Technology, 730050 Lanzhou, China

ARTICLE INFO

Keywords:
TWIP steel
Heterogeneous structure
Twin
High strength
Thermal stability

ABSTRACT

Twinning-induced plasticity (TWIP) steels can exhibit high ultimate strength and ductility, but low yield strength and thermal stability. Here we approach this problem by introducing a heterogeneous microstructure comprised of soft, hard and thermally stable regions in a model composition of Fe-22Mn-0.6 C TWIP steel. This target microstructure is achieved via a three-step processing route: cold rolling to introduce nanotwin bundles, an aging treatment to transform highly defective regions to thermally stable pearlite nano-lamellae, and an annealing step for relatively large, ductile grains. We show that this microstructure generates a good balance between high yield strength, good ductility, high ultimate tensile strength, and good thermal stability. The main deformation mechanism of this unique heterogeneous structure is deformation twinning. The high thermal stability can be attributed to the transformation of the shear bands, introduced by cold rolling, into pearlite during the aging process, and into the composite of nanograined austenite and nanograined cementite formed during the subsequent isothermal annealing.

1. Introduction

High-manganese, twinning-induced plasticity (TWIP) steels has attracted a great deal of attention in the automotive industry due to an outstanding combination of mechanical properties, such as high ultimate strength and high ductility [1,2]. One factor limiting the application of TWIP steels is, however, its relatively low yield strength, which varies from 200 MPa to 400 MPa [2,3]. High yield strength, at which the material begins to deform permanently, is particularly important for most of the frequently encountered service conditions, while high ultimate strengths and toughness, for example, are important for the infrequent situations, such as impacts, and the crash-relevant parts of the automobile. Therefore, improving the yield strength, while maintaining, at the same time, high ultimate strength, elongation-to-failure, and thermal stability of TWIP steels, is ideal.

Over the years many attempts to increase the properties of TWIP steels have been reported and they include compositional adjustments [4–9], precipitation strengthening [10], pre-straining by cold rolling [11,12], recovery and partial recrystallization of pre-strained sheet [13–17]. These methods either led to insufficient increases in yield strength or successfully increased the yield strength but with unacceptable losses in ductility and/or thermal stability.

One promising avenue to overcome these trade-offs is to design the TWIP steel material with a heterogeneous microstructure [18,19]. Heterogeneous structures can be regarded as a hybrid material composed of “hard domains”, providing the prominent strength, and “soft domains”, providing the ductility [18,19]. This class of material microstructure has proven to be effective in achieving the best combination of strength and ductility. Examples include bimodal grain-size distributions [20–22], gradient structures [23–25], bimetal laminate structures [26,27], dual-phase or multi-phase steels [28–30] and partially recrystallized structures [31–34]. Cold deformation plus partial recrystallization is the most common method to fabricate heterogeneous microstructure with single-phase materials [22,31,32]. However, the heterogeneous microstructure produced by these methods are thermally less stable [35]. The reason is that this type of heterogeneous microstructure comprises nano-grained regions containing high densities of grain boundaries and defects, which induce grain growth

* Corresponding author.
** Corresponding author at: Shenyang National Laboratory for Materials Science, Institute of Metal Research, Chinese Academy of Sciences, 72 Wenhua Road, Shenyang 110016, PR China.
E-mail addresses: sjzheng@imr.ac.cn (S.J. Zheng), xlma@imr.ac.cn (X.L. Ma).

https://doi.org/10.1016/j.msea.2018.02.003
Received 17 January 2018; Received in revised form 31 January 2018; Accepted 1 February 2018
Available online 15 February 2018
0921-5093/

during exposure to elevated temperatures, even for relatively short times (e.g., minutes).

Here we present an approach to produce a heterogeneous microstructure that exploits the desirable features manifesting at both the micron scale and the nanoscale in the same TWIP material. The key microstructural features span five orders of magnitude and combine the ductility benefits of large grains, and the thermal stability and high strength of coherent nanotwinned boundaries and nanosized metal-matrix ceramic lamellar composite grains. The proposed processing route to achieve this heterogeneous microstructure involves three steps: one mechanical and two thermal treatments that induce phase transformations. Microscopy reveal how each processing step relies on the prior one and leads to the target nanoscale features, and in turn, how each feature contributes to the intended structural performance.

2. Experimental procedures

The Fe-22Mn-0.6 C steel was cast in a medium frequency induction furnace using pure raw material powders (purity higher than 99.9 wt. %). The cast ingot was homogenized at 1150 °C for 2 h, then water quenched, and finally cold-rolled (at room temperature) to a 50% reduction in thickness. To reveal the effect of aging and annealing on the microstructure, cold-rolled samples with and without aging (–Ag) and with and without annealing (–A) were made. The aging step was performed at 400 °C for 336 h and the annealing step was done at 600 °C for either 5 or 10 mins (–A5 or –A10). The types of samples studied are summarized on Table 1.

From these samples, specimens were prepared and analyzed via transmission electron microscopy (TEM), scanning electron microscopy (SEM), and tensile testing. The TEM specimens were cut along the longitudinal direction of rolling. After mechanically grinding down to a thickness of ~100 μm, disks with a diameter of 3 mm were punched out from the thin foils. The disks were then subjected to a twin-jet electrochemical polishing in a solution of 5% perchloric acid and 95% ethanol at 25 V and a temperature of around − 20 °C. TEM observation was performed in an FEI Tecnai G2 F30 transmission electron microscope, equipped with a high-angle angular-dark-field (HAADF) detector and X-ray energy-dispersive spectrometer (EDS) systems, operated at 300 kV.

To quantify the volume fraction of each region (nanotwinned bundles, shear bands, etc) in each sample, SEM was performed in the normal direction (ND) plane in both the transverse direction (TD) and rolling direction (RD). The scanning electron microscope used a Hitachi SU-70 field emission gun (FEG-SEM) equipped with a low-voltage, high-contrast detector (vCD) for the backscattered electron (BSE) mode. To get representative data from the image analysis, areas in an range from ~ 0.6 mm × 0.25 mm to ~1.5 mm × 2.5 mm for different samples were analyzed using the Image J software (available at http://rsb.info.nih.gov/ij). The SEM images are not shown for brevity.

The effect of microstructural differences due to the intermediate aging step on mechanical performance was evaluated by tensile testing. Uniaxial tensile testings of the two sets of samples were performed on a universal testing machine at room temperature with a nominal strain rate of 5×10^{-4} s^{-1}. All tensile specimens were flat and dog-bone-shaped with a gauge length of 12 mm, a width of 2 mm, and a thickness of 2.4 mm. The longitudinal axes of the tensile specimens were parallel to the rolling direction. Moreover, the strain less than 5% was measured by extensometer. After the tensile testings, TEM specimens were cut from the gauge sections along the load direction.

Table 1
Specific processing parameter of the two sets of samples.

Cold rolling reduction in thickness	Aging treatment	Annealing time (minutes) at 600 °C	Referred to as
50%		—	CR
	—	5	CR-A5
		10	CR-A10
		—	CR-Ag
	400 °C/336 h	5	CR-Ag-A5
		10	CR-Ag-A10

3. Results

SEM and TEM analyses found that all the thermomechanical schedules in Table 1 created samples with heterogeneous structures comprised of both micron and nanoscale microstructural features.

First, the microstructure of the sample in the cold-rolled initial state after 50% reduction (CR), before partial recrystallization and aging, is studied via SEM and TEM. Nanotwin bundles and shear bands are typical deformation structures of TWIP steel subjected to cold rolling [36]. Consistent with prior studies, many nanotwin bundles and shear bands formed as a result of the deformation as shown in Fig. 1(a). Statistical SEM analysis, finds the volume fractions of the twin bundles (NT) and shear bands (SB), in the cold rolled sample, are ~84%, and ~16%, respectively.

Fig. 2(a) is a typical transmission electron microscopy (TEM) image of the nanotwin bundles in the CR sample. These nanotwins bear a high density of dislocations at the twin boundaries (TBs) and within the alternating twin/matrix (T/M) lamellae. The cold rolling induced unstable shear bands. TEM analysis finds that the shear bands crossed the NT bundles. Fig. 2(b) is an image of a typical shear band about 200 nm thick intersecting the T/M lamellae. This band, like the others, is comprised of weakly textured, nano-sized grains, as indicated by the SAED pattern at the top right.

Next we examine the microstructure after cold rolling and the aging step (R-A). Fig. 3(a) is a typical bright-field TEM image of this R-A sample. From analysis of 100 images, two regions bearing nanoscale structures are frequently seen: 1) nanotwin bundles and 2) a lamellar structure. Based on the SAED pattern (Fig. 3(b)), the latter region is indexed as a composite SAED of [111]-oriented α-ferrite and [010]-oriented $(Fe, Mn)_3C$ cementite. The orientation relationship (OR) between α ferrite and $(Fe, Mn)_3C$ cementite is: α [111] // $(Fe, Mn)_3C$ [010] and α $(0\bar{1}1)$ // $(Fe, Mn)_3C$ $(10\bar{3})$, which is the well-known Isaichev OR between ferrite and cementite [37,38]. The two-phase pearlite region is the consequence of the decomposition of the austenite phase during aging. The EDS results (Fig. 4) indicate the darker and thinner lamella is cementite enriched with Fe, Mn, C, and the brighter and thicker lamella is α-ferrite enriched with Fe. The average thicknesses of the α-ferrite and cementite lamellae (based on 100 lamellae) are 27.5 ± 10.3 nm and 47.6 ± 20.6 nm, respectively.

Another interesting finding is that the aging step removes the shear bands. It can be inferred that shear bands were transformed into pearlite colonies since the distribution and shape of the pearlite colonies in CR-Ag samples (Fig. 1(d) are basically the same as those of the shear bands in the CR sample (Fig. 1(a)). The excess energy stored in the shear bands contfaining high density high-angle grain boundaries is much higher than that in the twin bundles [39]. Meanwhile, it has been reported that pearlite prefers to nucleate in the regions of high-energy defect storage [40]. The volume fraction of the pearlite is ~21% according to statistical measure from SEM images, which is larger than the volume fraction of the shear bands before aging treatment. Taken together, while the CR and CR-Ag samples are both heterogeneous, consisting of nanotwinned bundles and relatively larger grains, the annealed structure of the CR-Ag has much more pearlite and less defective shear bands.

Tensile testing was carried out on several samples of CR and CR-Ag. Fig. 5(a) and (b) show typical tensile engineering stress-strain curves of these samples. The curves show a high yield stress (MPa) but failure immediately after yielding. To summarize, these two samples, after just cold rolling, and also after cold rolling and the aging treatment, lacked ductility.

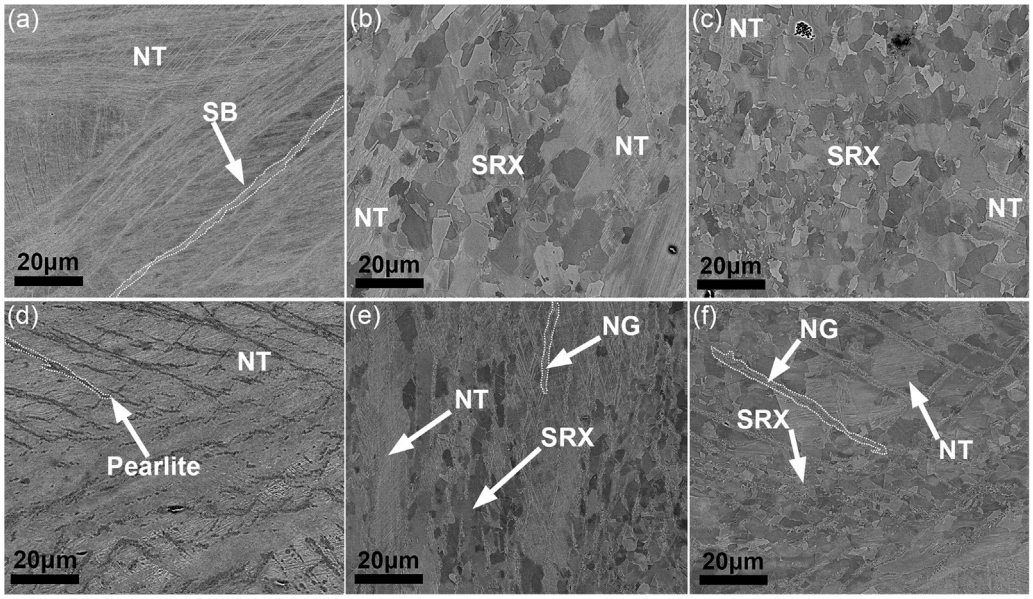

Fig. 1. Typical SEM images of the two sets of sample (a) the CR sample; (b) the CR-A5 sample; (c) the CR-A10 sample; (d) the CR-Ag sample; (e) the CR-Ag-A5 sample; (f) the CR-Ag-A10 sample.

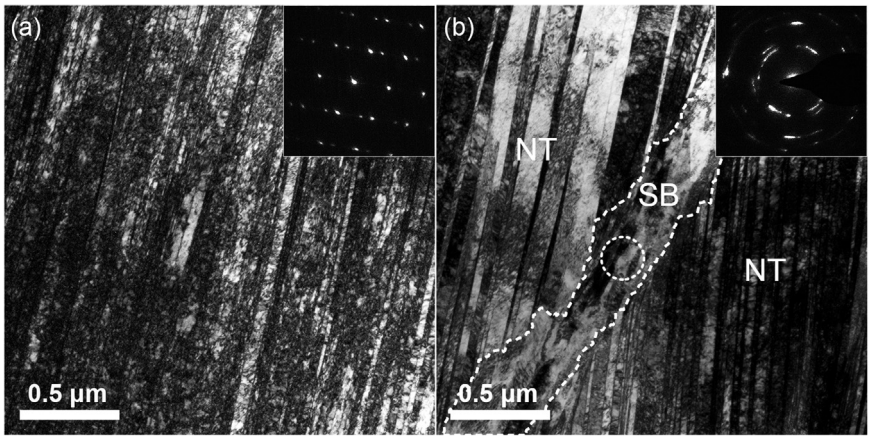

Fig. 2. Typical TEM images of CR sample: (a) a bright-field TEM image and its corresponding SAED pattern showing the existence of nanotwins; (b) a characteristic bright-field TEM image showing a shear band labeled as "SB" that intersects with the T/M lamellae, and a SAED pattern acquired from the white circle region.

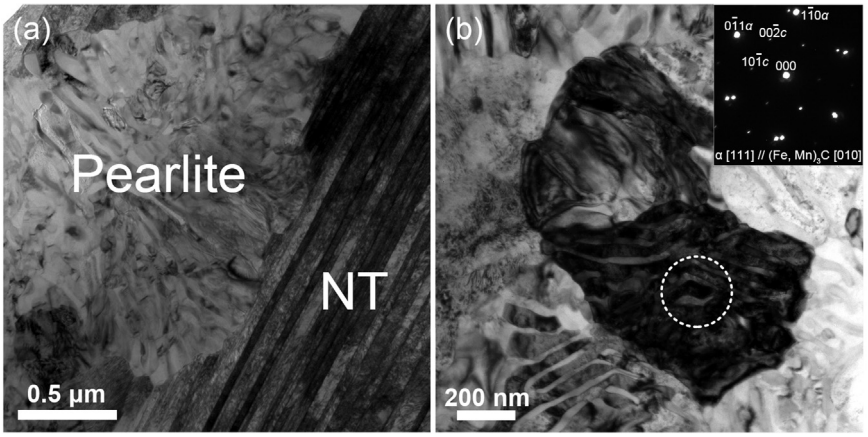

Fig. 3. (a) Characteristic TEM image of CR-Ag consisting of two regions: the nanotwin bundles region labeled as "NT" and the pearlite region. (b) Microstructure of the pearlite region and the corresponding composite SAED of the [111] zone axis reflections of α ferrite and [010] zone axis reflections of $(Fe, Mn)_3$ C cementite.

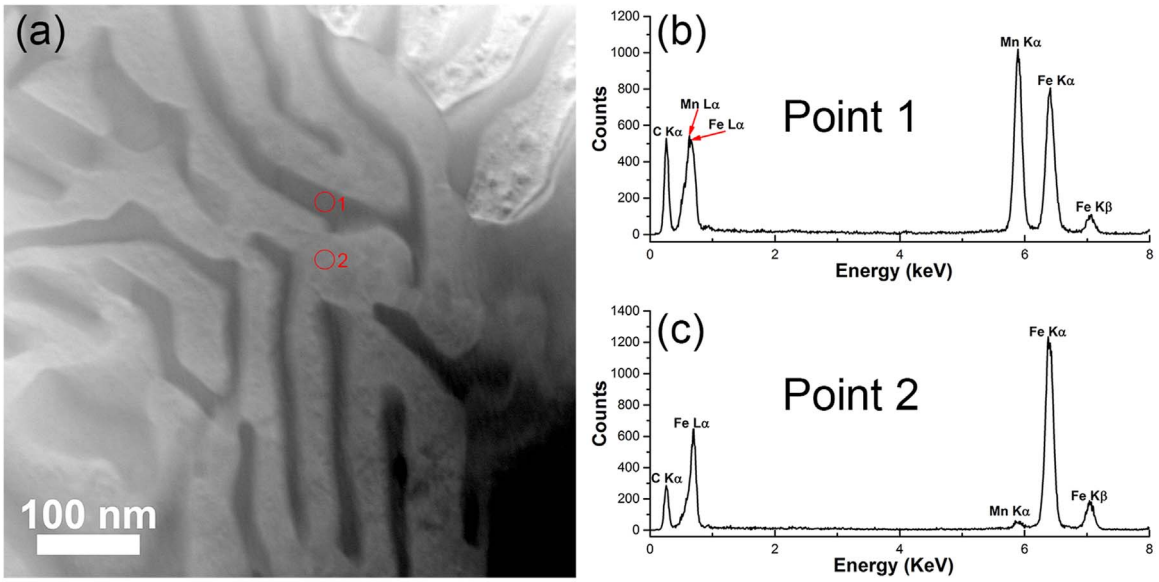

Fig. 4. (a) HAADF image showing the typical morphology of the lamellar pearlite. The numbers 1 and 2 are positions of the EDS measurements. (b) and (c) EDS displaying the composition of the points 1 and 2 in (b).

To establish the last reference, the microstructures of samples that were cold rolled and annealed for five or ten minutes (CR-A5 and CR-A10) were analyzed. In essence, the annealing step introduced micron-sized static recrystallization (SRX) grains into the cold-rolled structure. Fig. 1(b) and (c) show that the morphologies of these samples exhibit a small volume fraction of nanotwin bundles, remaining from the cold-rolled microstructure, embedded in micron-sized SRX grains. The shear bands formed during rolling, and parts of the nanotwin bundles, have been consumed by the growth of these SRX grains. With increasing annealing time from 5 mins to 10 mins, the volume fraction and the grain size of the SRX grains increase. Statistical analysis of SEM data indicates that the volume fractions of the SRX grains in CR-A5 and CR-A10 are ~56% and ~89%, respectively. The average sizes are 5.34 ± 3.06 μm and 6.56 ± 3.50 μm, respectively, for the CR-A5 and CR-A10 samples.

Tensile testing of CR-A5 and CR-A10 was performed to determine the influence of the SRX grains on the deformation response. The results are shown in Fig. 5(a). Compared to the CR samples, the strength decreases and ductility increases after annealing. The deformation microstructures contain high defect densities that tend to recrystallize too quickly during even the shortest annealing time, which usually leads to a great loss in strength. As a pertinent example, Tian et al. [35] demonstrated that when a cold rolled TWIP steel was annealed at 550 °C for only 4 mins, the yield strength dropped dramatically from 1810 MPa to 793 MPa.

Finally, the microstructures of the samples that were cold-rolled (CR), aged (Ag), and annealed (A5 or A10), denoted as CR-Ag-A5 and CR-Ag-A10, were studied using TEM and SEM. Unlike the other samples that were rolled only, rolled and aged only or rolled and annealed only, these samples had the desired multi-phase heterogeneous structure. Three distinct regions characterize this new structure: micro-grained SRX grain region, NT bundles region, and nano-sized grain region.

Fig. 1(e), (f) and Fig. 6(a) show typical SEM and TEM images of these samples. As shown, parts of the NT bundles transform into soft microcrystalline SRX grains. According to SEM statistical analysis, the volume fraction and grain size of the SRX grains increase with the increasing annealing time from 5 to 10 mins. The SRX grain volume fractions are ~22% in CR-Ag-A5 and ~35% in CR-Ag-A10, respectively, and the concomitant SRX grain sizes are 3.54 ± 2.07 μm and 5.27 ± 3.51 μm.

During annealing, the pearlite region that formed during the aging treatment spheroidizes and evolves into a dual-phase region mixed with nano-sized grains of austenite and cementite. Fig. 6(b) shows a typical TEM observation, with their corresponding SAEDs, of this mixed nano-

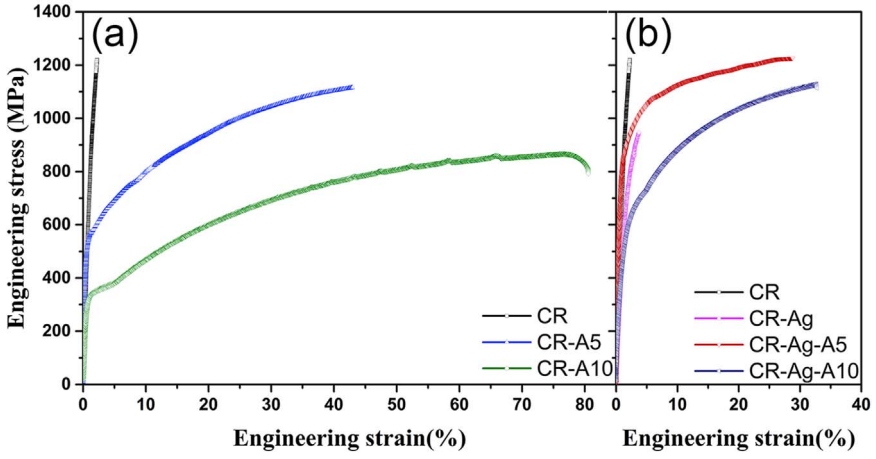

Fig. 5. Tensile engineering stress-strain curves of (a) the cold rolled set of samples; (b) the aged set of samples.

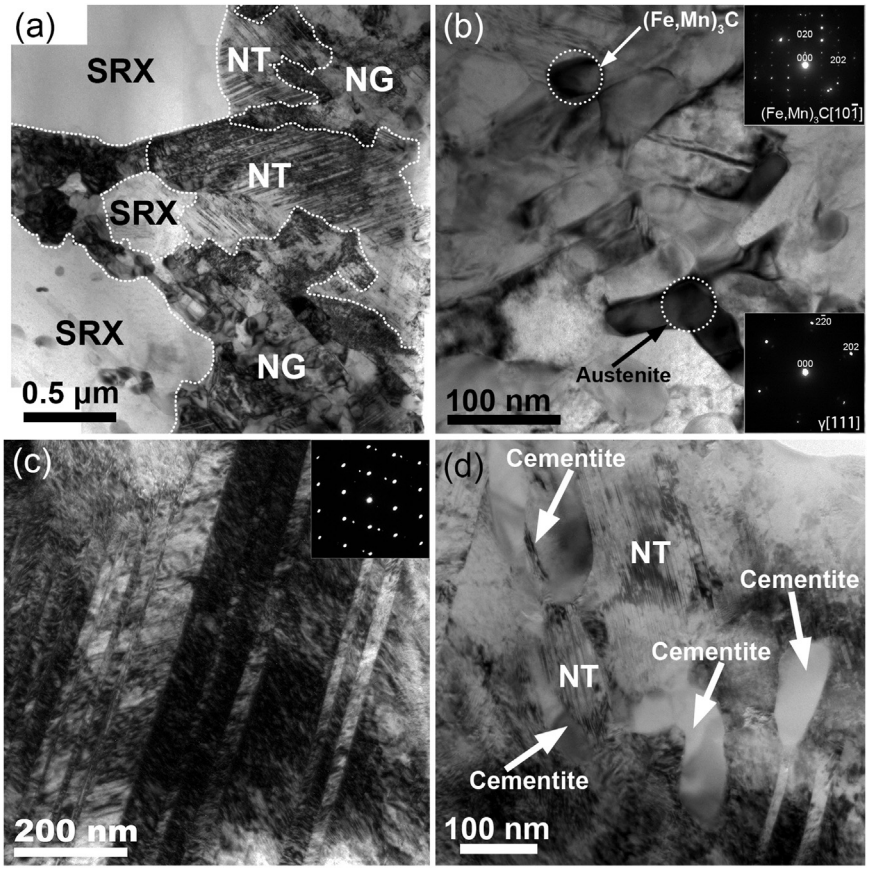

Fig. 6. (a) A typical TEM image of a CR-Ag-A5 sample, showing a multi-phase heterogeneous structure consisting of three typical regions: micro-grained SRX grain region, nanotwin bundles region (labeled as NT), and nano-sized grain region (labeled as NG). (b) A close TEM observation of the nano-sized grain region showing elliptical cementite (Fe, Mn)$_3$ C and polygonal γ austenite and their corresponding SAED inserted. Typical bright-field TEM images of the CR-Ag-A5 sample after tensile testing (c) showing the nanotwin bundles with high density of dislocations and the corresponding SAED; (d) showing un-deformed cementite labeled with white arrows and nanotwin bundles labeled as "NT" with thinner and denser twin lamellae.

sized grain region, comprised of elliptical-shaped cementite and polygonal-shaped austenite. The volume fraction of the nano-sized grain region remains unchanged with increasing annealing time, accounting for 18% volume fraction. Meanwhile, the average grain sizes of austenite and cementite increase slightly from 220.44 ± 74.10 nm to 254.13 ± 78.72 nm and from 66.10 ± 22.73 nm to 72.50 ± 24.11 nm, respectively.

Tensile testing of CR-Ag-A5 and CR-Ag-A10 was used to determine the deformation response of this heterogeneous structure. Fig. 5(b) shows typical tensile engineering stress-strain curves. For CR-Ag-A5 sample, the yield strength, ultimate strength, and elongation-to-fracture were 850 MPa, 1200 MPa and 28%. Comparatively, in the CR-Ag-A10 sample, the yield and ultimate strength decrease and the ductility increases slightly. The sample CR-Ag-A5 exhibits the best mechanical performance in all the samples studied.

To determine the deformation mechanisms underlying the tensile response, TEM was used to characterize the microstructure of the CR-Ag-A5 sample after tensile testing, two morphological changes were found. First, micron-sized bundles of nanotwins, containing a high density of dislocations (Fig. 6(c)) were found, in greater volume fraction than that in the sample before tensile testing. It is envisioned that the micron-sized SRX grains deformed via twinning during the tensile testing. Second, the nano-sized grain region dramatically evolves. While the elliptical shaped, nano-sized cementite remains un-deformed, as labeled with white arrows in Fig. 6(d), the nano-sized austenite has transformed into nanotwin bundles with thinner and denser nanoscale lamellae than those in the micrometer sized grains (Fig. 6(c)), as labeled with NT in Fig. 6(d). These results indicate that twinning is a major deformation mechanism in the optimized heterogeneous structure.

4. Discussion

Incorporating the intermediate aging treatment enhanced the thermal stability of the TWIP steel. After the 5-min annealing, the volume fraction of the SRX accounts for ~56% in CR-A5, while it is only ~22% in CR-Ag-A5. When prolonged the annealing time to 10 mins, the volume fraction of the SRX grains accounts for ~89% in CR-A10, while its value just accounts for 35% in CR-Ag-A10. Besides, comparing the tensile properties of the CR-Ag-A10 sample and the R-A5 sample finds that the aged structure presents both higher yield strength and ultimate strength after the 10-min annealing than the cold-rolled structure after the 5-min annealing.

The enhancement in thermal stability caused by the aging treatment can be explained through its effect on the microstructure. First, aging causes a substitution of an unstable, high-energy deformed structure with a thermally stable one. For TWIP steels with low SFEs, typical deformation structures such as twin bundles and shear bands, would be induced by pre-straining [36]. Static recrystallization preferentially occurs in the shear band region due to its high excess energy [31]. During the aging treatment, however, the high-energy shear bands were substituted by laminar pearlite, and then in the subsequent annealing treatment, this region transformed into a region mixed with nano-sized cementite and austenite grains. In this mixed dual-phase structure, most of the grain boundaries between the two phases can be pinned significantly retarding their movement [41]. As a result, the grain sizes of austenite and cementite within the nano-sized region will grow slowly during the annealing process. Finally, another important reason is that the aging treatment at 400 ℃ could have also recovered some of the dislocations that had accumulated within the nanotwin bundles. It has also been reported that dislocation density could be reduced by the aging treatment [42,43].

It is realized that adding the intermediate aging treatment provides the desired thermal stability, while, it extends the overall material

processing time. Future attention could be paid to optimizing the intermediate aging process to attain the target thermal stability for the minimum aging time.

The high strength of the heterogeneous TWIP steel made here originates from the two harder regions of the microstructures: the nanotwin bundles and the nanograin regions, with volume fractions of 60% and 18%, respectively. Within the nanotwin bundles, the twin boundaries are strong obstacles to the movement of dislocations [44]. The strength of the twin bundles can reach ~2.0 GPa according to previous reports [31]. According to the Hall-Petch effect, the nano-sized grain region, containing a mix of nanograins of austenite, also contributes to the high strength. Within the nanograin regions, the austenite/cementite interface provides another obstacle for dislocation motion, which is also an important strengthening mechanism, as has been extensively demonstrated in steels [45,46].

Comparing the microstructure evolution and tensile properties of the two sets of samples, we can conclude that adding the intermediate aging treatment decreases speed of recrystallization that transforms the deformed structure into SRX grains. The SRX grains can give rise to the trade-off in strength and ductility seen in conventional metals, leading to a weaker material while extending ductility. The heterogeneous microstructure created by adding the intermediate aging treatment delays the softening of the material.

The micron-sized SRX grains are responsible for the relative high ductility. They have good ductility with an elongation-to-fracture about 80% according to the CR-A10 sample with almost full recrystallization structure. The microstructure of the heterogeneous TWIP steel shown by TEM observation reveals that during the tensile testing both the SRX austenite and the nano-sized austenite in the nano-sized region deform mainly by twinning. Thus, the microstructure still exploits the characteristic TWIP effect in deformation, profusely activating nanoscale deformation twinning known to result in good ductility [47].

5. Conclusions

In summary, we present an approach for making a TWIP steel with an unusually highly heterogeneous microstructure, containing sizeable amounts of micron-sized austenite grains, nanotwin bundles, and nano-sized austenite/cementite composite grains. The manufacturing route involves cold rolling, an intermediate aging treatment, and final annealing step. The new heterogeneous structure enables a two-fold increase in yield (850 MPa) compared to TWIP steels, while remarkably maintaining a high ultimate tensile strength (1200 MPa), excellent thermal stability (compared with its traditional TWIP counterpart), and a uniform elongation of 28%. The possible mechanisms responsible for the microstructural changes resulting from each processing step are discussed. The high thermal stability comes from substitution of unstable shear bands with stable laminar pearlite and then mixed with nano-sized cementite and austenite grains. Testing and microscopy analysis find that the main deformation mechanism of this unique heterogeneous structure is deformation twinning.

Acknowledgements

S. Z. gratefully acknowledges support for this research by “Hundred Talents Project” of Chinese Academy of Sciences, “Thousand Youth Talents Plan” of China, National Natural Science Foundation of China (grant number 51401208, 51771201), and Shenyang National Laboratory for Materials Science (grant number 2015RP18, 2017RP17). I.J.B. acknowledges financial support from the National Science Foundation program (NSF CMMI-1729887). The authors also would like to thank D. L. Wang, B. Wu, and G. Xie for their technical support.

References

[1] O. Grassel, L. Kruger, G. Frommeyer, L.W. Meyer, High strength Fe-Mn-(Al, Si) TRIP/TWIP steels development - properties - application, Int. J. Plast. 16 (10–11) (2000) 1391–1409.
[2] G. Frommeyer, U. Brux, P. Neumann, Supra-ductile and high-strength manganese-TRIP/TWIP steels for high energy absorption purposes, Isij Int. 43 (3) (2003) 438–446.
[3] O. Bouaziz, N. Guelton, Modelling of TWIP effect on work-hardening, Mater. Sci. Eng. A - Struct. 319 (2001) 246–249.
[4] J.E. Jin, Y.K. Lee, Effects of Al on microstructure and tensile properties of C-bearing high Mn TWIP steel, Acta Mater. 60 (4) (2012) 1680–1688.
[5] K. Jeong, J.-E. Jin, Y.-S. Jung, S. Kang, Y.-K. Lee, The effects of Si on the mechanical twinning and strain hardening of Fe–18Mn–0.6C twinning-induced plasticity steel, Acta Mater. 61 (9) (2013) 3399–3410.
[6] S. Liu, L.H. Qian, J.Y. Meng, D.D. Li, P.H. Ma, F.C. Zhang, Simultaneously increasing both strength and ductility of Fe-Mn-C twinning-induced plasticity steel via Cr/Mo alloying, Scr. Mater. 127 (2017) 10–14.
[7] K.G. Chin, C.Y. Kang, S.Y. Shin, S. Hong, S. Lee, H.S. Kim, K.H. Kim, N.J. Kim, Effects of Al addition on deformation and fracture mechanisms in two high manganese TWIP steels, Mater. Sci. Eng. A - Struct. 528 (6) (2011) 2922–2928.
[8] M. Ghasri-Khouzani, J.R. McDermid, Effect of carbon content on the mechanical properties and microstructural evolution of Fe-22Mn-C steels, Mater. Sci. Eng. A - Struct. 621 (2015) 118–127.
[9] S. Lee, J. Kim, S.J. Lee, B.C. De Cooman, Effect of Cu addition on the mechanical behavior of austenitic twinning-induced plasticity steel, Scr. Mater. 65 (12) (2011) 1073–1076.
[10] C. Scott, B. Remy, J.L. Collet, A. Cael, C.M. Bao, F. Danoix, B. Malard, C. Curfs, Precipitation strengthening in high manganese austenitic TWIP steels, Int. J. Mater. Res. 102 (5) (2011) 538–549.
[11] P. Kusakin, A. Belyakov, C. Haase, R. Kaibyshev, D.A. Molodov, Microstructure evolution and strengthening mechanisms of Fe-23Mn-0.3C-1.5Al TWIP steel during cold rolling, Mater. Sci. Eng. A - Struct. 617 (2014) 52–60.
[12] N.K. Tewary, S.K. Ghosh, S. Bera, D. Chakrabarti, S. Chatterjee, Influence of cold rolling on microstructure, texture and mechanical properties of low carbon high Mn TWIP steel, Mater. Sci. Eng. A - Struct. 615 (2014) 405–415.
[13] O. Bouaziz, C.P. Scott, G. Petitgand, Nanostructured steel with high work-hardening by the exploitation of the thermal stability of mechanically induced twins, Scr. Mater. 60 (8) (2009) 714–716.
[14] O. Bouaziz, D. Barbier, P. Cugy, G. Petigand, Effect of process parameters on a metallurgical route providing nano-structured single phase steel with high work-hardening, Adv. Eng. Mater. 14 (1–2) (2012) 49–51.
[15] O. Bouaziz, D. Barbier, Benefits of recovery and partial recrystallization of nano-twinned austenitic steels, Adv. Eng. Mater. 15 (10) (2013) 976–979.
[16] C. Haase, T. Ingendahl, O. Guvenc, M. Bambach, W. Bleck, D.A. Molodov, L.A. Barrales-Mora, On the applicability of recovery-annealed Twinning-Induced Plasticity steels: potential and limitations, Mater. Sci. Eng. A - Struct. 649 (2016) 74–84.
[17] P. Zhou, Z.Y. Liang, R.D. Liu, M.X. Huang, Evolution of dislocations and twins in a strong and ductile nanotwinned steel, Acta Mater. 111 (2016) 96–107.
[18] X. Wu, Y. Zhu, Heterogeneous materials: a new class of materials with unprecedented mechanical properties, Mater. Res. Lett. 5 (8) (2017) 527–532.
[19] E. Ma, T. Zhu, Towards strength-ductility synergy through the design of heterogeneous nanostructures in metals, Mater. Today 20 (6) (2017) 323–331.
[20] Y.M. Wang, M.W. Chen, F.H. Zhou, E. Ma, High tensile ductility in a nanostructured metal, Nature 419 (6910) (2002) 912–915.
[21] Y.M. Wang, E. Ma, Three strategies to achieve uniform tensile deformation in a nanostructured metal, Acta Mater. 52 (6) (2004) 1699–1709.
[22] X. Wu, M. Yang, F. Yuan, G. Wu, Y. Wei, X. Huang, Y. Zhu, Heterogeneous lamella structure unites ultrafine-grain strength with coarse-grain ductility, Proc. Natl. Acad. Sci. USA 112 (47) (2015) 14501–14505.
[23] T.H. Fang, W.L. Li, N.R. Tao, K. Lu, Revealing extraordinary intrinsic tensile plasticity in gradient nano-grained copper, Science 331 (6024) (2011) 1587–1590.
[24] Y.J. Wei, Y.Q. Li, L.C. Zhu, Y. Liu, X.Q. Lei, G. Wang, Y.X. Wu, Z.L. Mi, J.B. Liu, H.T. Wang, H.J. Gao, Evading the strength- ductility trade-off dilemma in steel through gradient hierarchical nanotwins, Nat. Commun. 5 (2014).
[25] H.T. Wang, N.R. Tao, K. Lu, Architectured surface layer with a gradient nanotwinned structure in a Fe–Mn austenitic steel, Scr. Mater. 68 (1) (2013) 22–27.
[26] S.J. Zheng, I.J. Beyerlein, J.S. Carpenter, K.W. Kang, J. Wang, W.Z. Han, N.A. Mara, High-strength and thermally stable bulk nanolayered composites due to twin-induced interfaces, Nat. Commun. 4 (2013).
[27] I.J. Beyerlein, J.R. Mayeur, S.J. Zheng, N.A. Mara, J. Wang, A. Misra, Emergence of stable interfaces under extreme plastic deformation, Proc. Natl. Acad. Sci. USA 111 (12) (2014) 4386–4390.
[28] Z. Li, K.G. Pradeep, Y. Deng, D. Raabe, C.C. Tasan, Metastable high-entropy dual-phase alloys overcome the strength–ductility trade-off, Nature (2016).
[29] M. Calcagnotto, Y. Adachi, D. Ponge, D. Raabe, Deformation and fracture mechanisms in fine- and ultrafine-grained ferrite/martensite dual-phase steels and the effect of aging, Acta Mater. 59 (2) (2011) 658–670.
[30] B.B. He, B. Hu, H.W. Yen, G.J. Cheng, Z.K. Wang, H.W. Luo, M.X. Huang, High dislocation density-induced large ductility in deformed and partitioned steels, Science 357 (6355) (2017) 1029–1032.
[31] F.K. Yan, G.Z. Liu, N.R. Tao, K. Lu, Strength and ductility of 316L austenitic stainless steel strengthened by nano-scale twin bundles, Acta Mater. 60 (3) (2012) 1059–1071.
[32] G. Dini, A. Najafizadeh, R. Ueji, S.M. Monir-Vaghefi, Improved tensile properties of partially recrystallized submicron grained TWIP steel, Mater. Lett. 64 (1) (2010) 15–18.
[33] D.B. Santos, A.A. Saleh, A.A. Gazder, A. Carman, D.M. Duarte, É.A.S. Ribeiro,

B.M. Gonzalez, E.V. Pereloma, Effect of annealing on the microstructure and mechanical properties of cold rolled Fe–24Mn–3Al–2Si–1Ni–0.06C TWIP steel, Mater. Sci. Eng. A 528 (10–11) (2011) 3545–3555.
[34] J. Zhang, D. Raabe, C.C. Tasan, Designing duplex, ultrafine-grained Fe-Mn-Al-C steels by tuning phase transformation and recrystallization kinetics, Acta Mater. 141 (2017) 374–387.
[35] Y.Z. Tian, Y. Bai, M.C. Chen, A. Shibata, D. Terada, N. Tsuji, Enhanced strength and ductility in an ultrafine-grained Fe-22Mn-0.6C austenitic steel having fully recrystallized structure, Metall. Mater. Trans. A 45 (12) (2014) 5300–5304.
[36] S. Vercammen, B. Blanpain, B.C. De Cooman, P. Wollants, Cold rolling behaviour of an austenitic Fe–30Mn–3Al–3Si TWIP-steel: the importance of deformation twinning, Acta Mater. 52 (7) (2004) 2005–2012.
[37] M. Guziewski, S.P. Coleman, C.R. Weinberger, Atomistic investigation into the atomic structure and energetics of the ferrite-cementite interface: the Bagaryatskii orientation, Acta Mater. 119 (2016) 184–192.
[38] A.A. Saleh, G. Casillas, E.V. Pereloma, K.R. Carpenter, C.R. Killmore, A.A. Gazder, A transmission Kikuchi diffraction study of cementite in a quenched and tempered steel, Mater. Charact. 114 (2016) 146–150.
[39] H.L. Wang, Z.B. Wang, K. Lu, Interfacial diffusion in a nanostructured Cu produced by means of dynamic plastic deformation, Acta Mater. 59 (4) (2011) 1818–1828.
[40] R.T. van Tol, L. Zhao, J. Sietsma, Kinetics of austenite decomposition in manganese-based steel, Acta Mater. 64 (2014) 33–40.
[41] F. Danan, L.Q. Chen, Computer simulation of grain growth and Ostwald ripening in alumina-zirconia two-phase composites, J. Am. Ceram. Soc. 80 (7) (1997) 1773–1780.
[42] G.W. Yuan, M.X. Huang, Supper strong nanostructured TWIP steels for automotive applications, Prog. Nat. Sci. -Mater. 24 (1) (2014) 50–55.
[43] F.K. Yan, N.R. Tao, K. Lu, Tensile ductility of nanotwinned austenitic grains in an austenitic steel, Scr. Mater. 84–85 (2014) 31–34.
[44] L. Lu, Y.F. Shen, X.H. Chen, L.H. Qian, K. Lu, Ultrahigh strength and high electrical conductivity in copper, Science 304 (5669) (2004) 422–426.
[45] M.D. Mulholland, D.N. Seidman, Nanoscale co-precipitation and mechanical properties of a high-strength low-carbon steel, Acta Mater. 59 (5) (2011) 1881–1897.
[46] T. Ohmura, T. Hara, K. Tsuzaki, H. Nakatsu, Y. Tamura, Mechanical characterization of secondary-hardening martensitic steel using nanoindentation, J. Mater. Res. 19 (1) (2004) 79–84.
[47] S. Allain, J.P. Chateau, O. Bouaziz, Constitutive model of the TWIP effect in a polycrystalline high manganese content austenitic steel, Steel Res. 73 (6–7) (2002) 299–302.